Analyst

ROYAL SOCIETY OF CHEMISTRY

MINIREVIEW

View Article Online
View Journal | View Issue

Cite this: *Analyst*, 2026, **151**, 973

MXene-based fluorescent aptasensors: advances and prospects in diagnostics and environmental monitoring

Rajapriya Govindaraju and Jongsung Kim *

Received 4th September 2025,
Accepted 16th January 2026

DOI: 10.1039/d5an00945f

rsc.li/analyst

MXene-based fluorescent aptasensors leverage the synergistic integration of the intrinsic physicochemical properties of MXenes, including tunable surface chemistry, broad-spectrum optical absorption, and superior fluorescence quenching efficiency, with the molecular recognition capabilities and strong binding affinity of aptamers. These two-dimensional transition metal carbides and nitrides efficiently suppress background fluorescence in dye-labeled aptamer systems through electrostatic interactions and π–π stacking. In the absence of the target analyte, the aptamers adsorb onto the MXene surface, facilitating non-radiative energy transfer and thereby suppressing the signal. Upon specific target recognition, a conformational rearrangement of the aptamer reduces its surface affinity, leading to desorption and subsequent fluorescence recovery *via* a target-induced "signal-on" mechanism. Such platforms demonstrate ultra-low detection limits, excellent selectivity, and modular adaptability for the detection of a broad spectrum of analytes, including clinical biomarkers, pathogenic microorganisms, environmental toxins, and heavy metal ions. This comprehensive review systematically summarises the mechanistic foundations of MXene–aptamer interactions, recent advancements in analytical applications, and emerging directions for translational development in biomedical diagnostics and environmental monitoring.

1. Introduction

Fluorescence-based biosensing has emerged as a powerful analytical approach for the detection and quantification of a wide range of analytes due to its high sensitivity, rapid response, and ease of operation. Fluorescent sensors function by transducing molecular recognition events into measurable optical signals, typically through changes in fluorescence intensity,[1] emission and excitation wavelength shift,[2] Förster resonance energy transfer (FRET) efficiency,[3] or fluorescence lifetime.[4] Among diverse fluorescence-based biosensing modalities, aptamer-functionalized fluorescent sensors (aptasensors) have emerged as highly promising platforms owing to the intrinsic high-affinity molecular recognition properties of aptamers combined with tunable fluorescence transduction mechanisms.[5] Aptamers, comprising synthetic single-stranded DNA or RNA sequences, are generated through SELEX processes to exhibit exceptional binding specificity and affinity toward a wide range of analytes.[6] Upon target interaction, aptamers frequently undergo conformational rearrangements or perturb the local microenvironment, leading to fluorescence signal modulation. This interplay enables the design of highly sensitive, selective, and often label-free or signal-enhanced fluorescence-based biosensors. Owing to their versatile target range, which includes small molecules, proteins, peptides, metal ions, and whole cells, fluorescent aptasensors represent a promising class of molecular tools for diagnostics, environmental monitoring, food safety, and biomedical research. The fluorescence signal change, triggered by aptamer–analyte interaction, provides a quantifiable output that can be correlated to the analyte concentration, offering a robust and precise detection strategy.

Two-dimensional (2D) nanomaterials have emerged as a prominent class of materials in sensing technologies, attributed to their atomically thin structures, high aspect ratios, and tunable surface chemistries.[7] Representative 2D materials, including graphene, transition metal dichalcogenides (TMDs), black phosphorus (BP), hexagonal boron nitride (h-BN), and MXenes, have demonstrated strong potential for interacting with diverse analytes and external stimuli, thereby facilitating highly sensitive and selective transduction mechanisms. The incorporation of these materials into aptamer-based biosensing platforms yields significant advantages. Their large specific surface area enables high-density aptamer immobilization,[8] which increases the probability of target recognition events and enhances signal response and dynamic range. Furthermore, aptamers, short single-stranded DNA or RNA sequences, form stable conjugates with 2D materials *via* π–π

Department of Chemical, Biological, and Battery Engineering, Gachon University, 1342 Seongnam-daero, Seongnam-si, Gyeonggi-do 13120, Republic of Korea.
E-mail: jongkim@gachon.ac.kr; Fax: +82-31-750-8943; Tel: +82-10-2212-5361

stacking/hydrophobic interactions,[9] hydrogen bonding,[10] and non-covalent interactions,[11] ensuring robust surface anchoring and signal transduction.

2D materials also exhibit superior electronic conductivity, mechanical robustness, chemical inertness, and tunable surface chemistry, all of which are critical for the fabrication of high-performance biosensors. The inherent specificity and affinity of aptamers, coupled with the signal amplification capabilities of 2D materials, result in biosensors with enhanced signal-to-noise ratios, ultra-low detection limits, and excellent selectivity, often outperforming conventional antibody-based systems. The versatility of 2D material-based aptasensors has been demonstrated across multiple application domains, including clinical diagnostics, environmental monitoring,[12] food safety assessment,[13] and toxicology screening.[14] The synergistic combination of 2D nanomaterials with aptamer technology significantly advances the analytical performance of biosensors, offering a platform that is highly sensitive, specific, rapid, and adaptable to various analytical scenarios.[15] MXenes, a novel family of 2D transition metal carbides, nitrides, or carbonitrides, have garnered substantial interest in sensor development due to their intrinsic hydrophilicity, exceptional mechanical robustness, and high electrical conductivity, which collectively facilitate efficient signal transduction and biomolecular interfacing.[16–18] MXene contributes to target recognition through the presence of various functional groups such as –F, –OH, =O, and –Cl. These functional groups, along with their high surface area, impart MXene with a highly tunable and hydrophilic nature, enhancing its dispersibility and making it a highly compatible material in aqueous environments.[19] Since their emergence, MXenes have been widely applied as sensing probes in both electrochemical and fluorescence-based detection platforms for the identification of metal ions, biomolecules, and toxins.[20] MXenes are utilized in both their sheet-like structures and as quantum dots, miniaturized versions of the original nanosheets, for the development of biosensing systems.[21,22] Their ability to undergo surface chemical modification makes MXene nanosheets particularly suitable for constructing aptamer-based sensors. Aptamers can be anchored onto the MXene surface, which serves as a transducer to enable sensitive and selective detection of target analytes. While MXenes have been extensively used in electrochemical aptasensors, their remarkable optical properties as strong near-infrared absorption,[23] excellent energy acceptor capabilities in energy transfer processes,[24] and effective fluorescence quenching,[25] make them highly promising for fluorescence-based aptasensor applications as well. The timeline for major milestones of MXene–aptamer-based sensors is shown in Fig. 1.

MXene-based fluorescence aptasensors offer several advantages, including strong fluorescence quenching ability, a high surface area with functional groups, enhanced biocompatibility, signal amplification, high sensitivity, and versatile functionalization. For instance, Yang *et al.* designed a signal-on fluorescent Nb_2C-MXene/B-CDs@Apt biosensor by integrating MXene with carbon dots (CDs), leveraging their strong fluorescence quenching properties.[26] Nb_2C-MXene, possessing a loose accordion-like nanostructure, was synthesized as an effective nanoquencher for B-CDs@Apt sensing, efficiently quenching fluorescence by adsorbing the DNA component of B-CDs@Apt. Additionally, a comparison was made between multilayer Nb_2C-MXene/B-CDs@Apt and monolayer Nb_2C/B-CDs@Apt in the development of a paper-based OTC biosensor. The monolayer Nb_2C/B-CDs@Apt paper-based

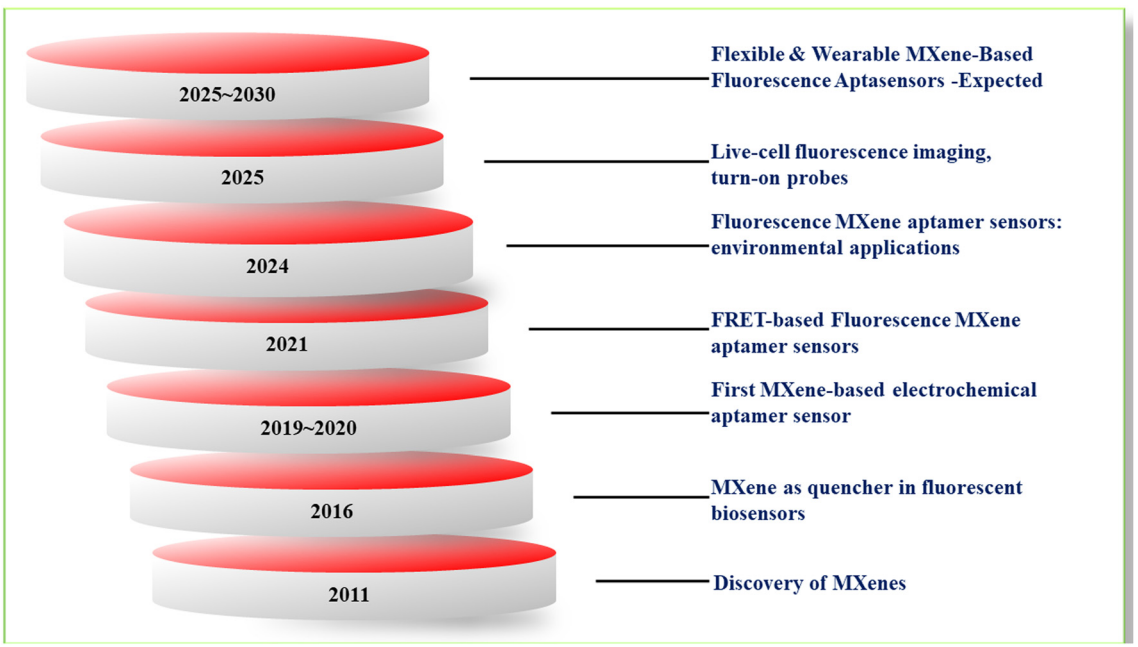

Fig. 1 Timeline for major milestones of MXene in aptamer-based sensing.

sensor exhibited lower sensitivity, reduced maximum fluorescence recovery, and a narrower detection range compared to its multilayer Nb_2C-MXene/B-CDs@Apt counterpart. Compared with conventional nanomaterials such as graphene oxide and MoS, MXenes exhibit superior charge-transfer kinetics and higher surface accessibility, resulting in enhanced sensitivity and faster response in electrochemical aptasensors. In optical sensing, particularly fluorescence-based platforms, $Ti_3C_2T_x$ MXenes demonstrate exceptional quenching efficiency *via* Förster resonance energy transfer and electron/energy transfer mechanisms, enabling highly responsive "signal-off/on" architectures governed by target-induced aptamer conformational changes. Functionalization of MXenes strongly affects the structural and electronic properties of the material; for instance, after surface passivation, a change in the band energy gap of the material greatly influences the absorption, reflection, and transition.[27] Table 1 represents the properties of MXene compared with other 2D materials. Collectively, these attributes establish MXenes as next-generation scaffolds for aptamer immobilization, delivering robust, ultrasensitive, and versatile sensing platforms for applications spanning clinical diagnostics, environmental monitoring, and food safety. Although several recent reviews have explored the role of MXenes in electrochemical aptasensing, a comprehensive overview of their potential in fluorescence-based aptasensors remains lacking. This review aims to address that gap by focusing on recent developments and the specific applications of MXenes in fluorescence-based aptasensing platforms. To keep the discussion engaging, we provide a concise overview of MXene synthesis and place greater emphasis on surface functionalization techniques, strategies for aptamer immobilization, and the diverse applications of these MXene–aptamer biohybrid systems in various sensing fields. The scope of this review encompasses: (i) a detailed overview of MXene structures and surface chemistries relevant to fluorescence modulation; (ii) mechanistic insights into fluorescence quenching pathways, including Förster Resonance Energy Transfer (FRET) and photo induced electron transfer; (iii) strategies for aptamers immobilization and functional interface engineering; and (iv) recent advancements in MXene-based aptasensing platforms for the detection of nucleic acids, proteins, small molecules, metal ions, and pathogenic organisms.

Table 1 Properties of MXene compared with other 2D materials

2D materials	Fluorescence quenching efficiency	Surface functional groups	Aptamer binding	Sensing mechanism	Biocompatibility	Ease of functionalization	Stability in biological media	Application example
MXene (*e.g.*, Ti_3C_2)	Very High (broad absorption range)	–OH, –F, =O (tunable)	Strong *via* electrostatic/π/π and H-bonding	FRET, IFE, turn-on/off, nonradiative energy transfer	Moderate to high	Moderate to high	Good (easily oxidizable)	Dopamine, thrombin, SARS-CoV-2, ATP
Graphene oxide (GO)	Highly efficient quenching	Carboxyl, epoxy, hydroxyl, carbonyl	Strong π–π and electrostatic	FRET, IFE	Good	Good	Excellent	miRNA, thrombin, cancer cells
MoS_2	Highly tunable quenching	(mainly edges)	S-terminated, possibly –OH, –C organic	FRET	Good	Moderate	Good	Glucose, DNA, ATP
Black phosphorus (BP)	High	P atoms (reactive); P–N, P–C bonds	Moderate	FRET, adsorption	Low	Poor	Poor	miRNA, antibiotics
h-BN (hexagonal boron nitride)	Low	Chemically inert	Poor	Static quenching	Excellent	Poor	Excellent	Dopamine, nicotine

2. Fundamentals of fluorescent aptasensors

2.1. Aptamer basics: selection, structure, and target recognition

Aptamers are short, single-stranded DNA or RNA oligonucleotides that serve as high-affinity molecular recognition elements, offering chemically stable and synthetically programmable alternatives to antibody-based receptors.[28] They are predominantly identified through Systematic Evolution of Ligands by Exponential Enrichment (SELEX), an *in vitro* Darwinian selection process originally introduced by Tuerk

and Gold, which iteratively enriches nucleic acid sequences exhibiting strong target specificity and affinity through cycles of binding, partitioning, and amplification. Molecular recognition is governed by the formation of well-defined secondary and tertiary aptamer structures, stabilized through non-covalent interactions,[28] enabling selective binding across a broad spectrum of targets from small organic molecules,[29,30] metal ions,[31,32] and peptides,[33] to large biomacromolecules such as proteins[34] and even entire cells.[35,36] Compared with antibodies, aptamers offer distinct advantages, including target-induced conformational adaptability, low immunogenicity, high chemical and thermal stability, scalable *in vitro* synthesis, and excellent batch-to-batch reproducibility, making them particularly attractive for biosensing applications. Although conventional SELEX protocols are often time-intensive, a series of advanced methodologies such as Cell-SELEX,[37] Artificially Expanded Genetic Information Systems (AEGIS)-SELEX,[38] Capillary Electrophoresis SELEX (CE-SELEX),[39] Microfluidic (Chip-Based) SELEX,[40] and more recently, computational and deep learning–assisted SELEX[41] have been developed to enhance selection efficiency, reduce turnaround time, and expand the chemical and structural diversity of aptamer libraries. Collectively, these next-generation SELEX platforms significantly accelerate the selection cycle while improving affinity, specificity, and structural versatility, thereby enabling the rapid development of high-performance aptamers for applications in diagnostics, targeted therapeutics, environmental monitoring, and nanobiotechnology.

2.2. Fluorescence principles: quenching, FRET, PET, and signal mechanisms

Aptamer-based fluorescence sensing platforms leverage the unique structural dynamics of aptamers upon target binding to modulate fluorescence output. These systems typically operate *via* three principal mechanisms: Förster Resonance Energy Transfer (FRET), contact quenching/dequenching, and photoinduced electron transfer (PET). FRET-based aptasensors are particularly favoured due to their high sensitivity to nanoscale conformational changes. In this approach, a fluorophore pair (donor and acceptor) is site-specifically attached to the aptamer. Target-induced folding alters the inter-fluorophore distance, modulating energy transfer efficiency. Proximity between the fluorophores enhances FRET (turn-on), while increased separation diminishes FRET, restoring donor emission (turn-off), thereby enabling quantitative detection of target analyte.[42]

Contact quenching (also known as quenching/dequenching) is another widely employed strategy in aptamer-based sensing.[43] In this approach, the fluorescence of a dye-labelled aptamer is suppressed by direct interaction with quenching agents, such as nucleotide bases or nanomaterials like gold nanoparticles, graphene oxide, MXenes, or MoS_2. Target engagement induces conformational rearrangements that either release the quencher or increase its distance from the fluorophore, thereby restoring fluorescence. This mechanism offers a straightforward and effective method for transducing binding events into optical signals. PET-based sensing involves the modulation of fluorescence *via* electron transfer processes.[44] Here, a fluorophore is covalently linked to the aptamer near an electron donor or acceptor moiety. In the unbound state, photoexcitation leads electron transfer, quenching the fluorophore. Upon target binding, the aptamer undergoes a structural change that disrupts the electron transfer pathway, leading to recovery of fluoroscence (turn-on). This strategy enables highly specific and sensitive detection based on precise spatial regulation of photoinduced electron dynamics.

3. Two-dimensional MXene nanomaterials

3.1. Structure and composition of MXenes

MXenes represent a family of two-dimensional (2D) transition metal carbides, nitrides, and carbonitrides, generally expressed by the formula $M_{n+1}X_nT_x$ (n = 1–4), where M denotes an early transition metal (*e.g.*, Ti, V, Nb, Mo), X is carbon and/or nitrogen, and T_x refers to surface terminations such as –OH, –O, –F, or –Cl. The integer n signifies the number of atomic X layers interleaved between adjacent M layers. MXenes are derived through the selective etching of the 'A' element, typically a group 13 or 14 element (*e.g.*, Al, Ga, Si)—from their MAX phase precursors with the general formula $M_{n+1}AX_n$. This top-down synthesis strategy removes the A element while retaining the layered M–X framework, resulting in a 2D material with a hexagonal close-packed lattice.[45] The resulting nanosheets exhibit a graphite-like layered morphology and are inherently terminated by functional groups originating from the etching medium, rendering them hydrophilic and chemically versatile. The final structure comprises ultrathin Ti_3C_2 layers functionalized with –OH, –O, and –F surface groups, which significantly influence their electronic structure, optical characteristics, and chemical reactivity. The compositional flexibility of MXenes is rooted in the vast number of available MAX phases, allowing for tunable combinations of M and X elements. To date, more than 50 MXene compositions have been experimentally realized, with over 100 stable structures predicted *via* first-principles calculations.[46] This high degree of tunability facilitates the design of MXenes with tailored physicochemical properties for specific functional applications. Altering the transition metal (M) enables control over electronic conductivity, magnetic behaviour, and electrocatalytic activity. Varying the carbon/nitrogen ratio (X) can modulate the mechanical stiffness, chemical stability, and electronic band structure.[47] Engineering the surface terminations (T_x) offers additional control over hydrophilicity, surface potential, interfacial chemistry, and optical responses, including fluorescence quenching efficiency.[48] Among these, surface terminations play a pivotal role in defining the interfacial interactions, electronic band alignment, and colloidal stability of MXene dispersions. These terminations not only influence the charge distribution and zeta potential but also govern criti-

cal properties such as bandgap modulation, aqueous stability, and photoactivity, which are crucial for applications in biosensing, photocatalysis, and energy conversion.[49] Moreover, post-synthetic modifications, such as thermal annealing, intercalation, or solvothermal treatments, offer further opportunities to fine-tune MXene composition and surface chemistry, thereby broadening their utility across diverse application domains, including electrochemical biosensors, energy storage devices, catalytic platforms, and optoelectronic systems.

3.2. Methods of synthesis and surface functionalization

MXenes can be synthesized *via* two principal methodologies: top-down and bottom-up approaches, each offering distinct advantages based on the targeted structural characteristics, surface functionalities, and application-specific requirements. In the top-down approach, MXenes are derived by the selective extraction of the 'A' element from their parent MAX phases ($M_{n+1}AX_n$). This is achieved through chemical or electrochemical etching techniques that preserve the integrity of the M–X layers while effectively removing the A-site atoms, thereby yielding 2D MXene nanosheets. Representative top-down methods includes direct hydrofluoric acid (HF) etching (*e.g.*, synthesis of $Ti_3C_2T_x$ from Ti_3AlC_2 using concentrated hydrofluoric acid),[50] *in situ* HF generation using fluoride salts and acids (*e.g.*, LiF + HCl),[51] molten salt etching (*e.g.*, Lewis acid etching with $ZnCl_2$),[52] and electrochemical etching (*e.g.*, anodic etching of Ti_3AlC_2 in an ionic electrolyte system).[53] This approach offers several advantages, such as high material yield, scalability, and effective A-layer removal. However, it is limited by drawbacks, including the use of hazardous reagents (*e.g.*, HF), limited control over the nature and density of surface terminations, and the restriction to synthetically accessible MAX phase precursors. The structure and synthesis strategies of MXenes derived from the MAX phase are illustrated in Fig. 2.

Conversely, the bottom-up approach entails the direct fabrication of MXene architectures from elemental or molecular precursors, bypassing the need for MAX phase templates. Techniques such as chemical vapor deposition (CVD),[54] template method,[55] and plasma-enhanced pulsed laser deposition (PELPD)[56] are employed to assemble MXene-like structures atom-by-atom or layer-by-layer. This method enables the synthesis of fluorine-free MXenes and offers precise control over stoichiometry, crystallographic orientation, and surface chemistry. Furthermore, it allows access to non-traditional MXene compositions that are not obtainable through conventional MAX-phase-based routes. Despite these advantages, bottom-up synthesis routes are often limited by low throughput, complex instrumentation requirements, high operational temperatures, and vacuum-dependent environments, which collectively hinder their scalability and cost-efficiency for large-scale production.

3.3. Optical, electronic, and surface properties of MXene

MXenes exhibit a broad spectrum of optical, electronic, and surface physicochemical properties, governed by their highly tunable chemical composition, layered 2D morphology, and diverse surface terminations. These characteristics endow

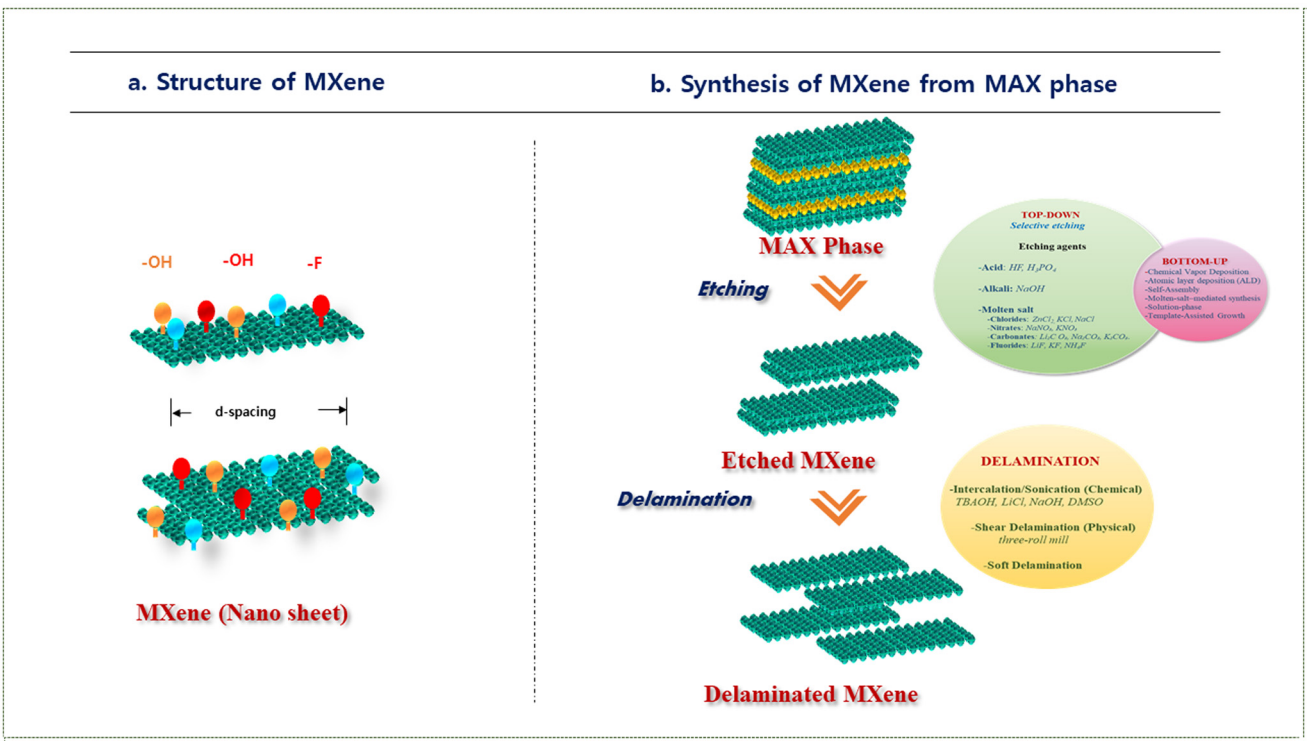

Fig. 2 Structure and synthesis of MXene from MAX phase.

MXenes with exceptional versatility across a wide range of application domains, including biosensing, photonic systems, catalysis, and electrochemical energy storage. Optically, MXenes demonstrate broadband absorption spanning the visible to near-infrared (NIR) regions, primarily due to intraband transitions and d–d electronic interactions within the transition metal layers. Certain MXenes exhibit strong photothermal conversion efficiencies under NIR irradiation,[57] making them excellent candidates for photothermal therapy and solar-driven applications. Additionally, some MXene compositions support localized surface plasmon resonance (LSPR) in the NIR region,[58] enabling plasmon-enhanced sensing, surface-enhanced Raman scattering (SERS), and light-harvesting applications.

From an electronic perspective, MXenes can exhibit either metallic or semiconducting behaviour, depending primarily on the composition of the transition metal (M), the X element (C or N), and the nature of the surface terminations (T_x). For example, MXene films have demonstrated high electrical conductivity, reaching values as high as 16 600 S cm^{-1}. However, post-synthetic surface modifications, particularly with –OH or –O functional groups, can induce bandgap opening, thereby transforming the material into a semiconducting state.[59] This tunable electronic property renders MXenes highly suitable for applications in field-effect transistors (FETs), optoelectronic devices, and photoelectrochemical sensors. The surface chemistry of MXenes plays a critical role in determining their aqueous stability, dispersion behaviour, and interfacial interactions. The abundant polar surface terminations (*e.g.*, –OH, –O) impart hydrophilicity and colloidal stability, enhancing their compatibility with biological environments. Moreover, these functional groups enable robust covalent and non-covalent conjugation with biomolecules, polymers, and nanostructures, facilitating the development of multifunctional hybrid systems for biosensing and nanomedicine.[60,61] Despite their outstanding functional properties, MXenes are inherently prone to oxidation, particularly under ambient or aqueous conditions. This degradation can be mitigated through antioxidant treatment, surface passivation, or storage in inert atmospheres. Furthermore, MXenes typically carry a net negative surface charge, which is advantageous for electrostatic interactions with positively charged analytes, supporting their integration in electrochemical and fluorescence-based biosensing platforms.

4. Strategies for aptamer immobilization on MXenes

MXenes have emerged as highly attractive two-dimensional platforms for the construction of nano–biohybrid biosensors due to their abundant surface-active sites, excellent aqueous stability, and favourable biocompatibility. Their broad optical absorption characteristics, combined with efficient electron- and energy-transfer properties, enable MXenes to function as powerful fluorescence quenchers while providing strong adsorption affinity toward diverse biorecognition elements, including enzymes, proteins, antigen–antibody systems, whole cells, and nucleic acid aptamers (DNA or miRNA). In MXene–aptamer sensing architectures, MXenes simultaneously act as signal transduction materials and immobilization scaffolds, thereby facilitating effective signal modulation. Depending on the sensing configuration, MXene surfaces may undergo activation or functionalization to enable aptamer attachment through either covalent coupling or non-covalent interactions.[62] In fluorescence-based sensing systems, however, aptamers are predominantly immobilized *via* physical adsorption rather than covalent linkage. A synergistic combination of electrostatic interactions governs this adsorption process, including π–π stacking between nucleobases and the MXene basal planes, hydrogen bonding, and van der Waals forces involving surface terminations (–O, –OH, and –F). Such non-covalent immobilization places fluorophore-labelled aptamers near the MXene surface, resulting in efficient fluorescence quenching. Upon target recognition, aptamer conformational rearrangements weaken the aptamer–MXene interaction, leading to partial desorption or increased spatial separation and consequent fluorescence recovery, thereby generating a characteristic "turn-on" sensing response, as schematically illustrated in Fig. 3.

As an example, Lin *et al.* introduced gold nanoparticle-decorated $Ti_3C_2T_x$ MXene nanosheets (MXene-Au) as effective quenchers for detecting deoxynivalenol (DON), a type of mycotoxin.[63] They designed luminescence resonance energy transfer (LRET) -based aptasensors by combining Er-doped upconversion nanoparticles (UCNPs) with MXene-Au nanohybrids. Their research primarily investigated the quenching efficiency of MXene-Au toward UCNPs. Notably, the emission spectrum of ssDNA-modified UCNPs overlapped well with the absorption spectrum of MXene-Au, enabling efficient LRET. Additionally, the distance between the donor (UCNPs) and acceptor (MXene-Au) is a key factor in triggering LRET. Due to their structural properties, ssDNA-UCNPs can readily approach MXene-Au, reducing the donor–acceptor distance and effectively quenching the luminescence. The UCL intensity of ssDNA-UCNPs gradually decreased as the concentration of MXene-Au increased. Furthermore, their findings showed that bare MXene had a lower quenching efficiency compared to MXene-Au, which enhances visible-light absorption and improves spectral overlap with the primary UCL emission peak of Er-UCNPs. Another interesting area of research explores variations in cellular ATP and GTP levels during mild photothermal therapy. Guan and their research team developed a fluorescent nanoprobe by modifying MXene with folic acid (FA)-PEG-NH_2 as a photothermal agent and integrating it with fluorescent aptamers.[64] This nanoprobe was designed to detect variations in ATP and GTP levels in both tumour and normal cells during mild photothermal therapy (mPTT). In this system, $Ti_3C_2T_x$ nanosheets were first carboxylated using chloroacetic acid. Then, through an amidation coupling reaction mediated by EDC and NHS, FA-PEG_{2000}-NH_2 was covalently attached to $Ti_3C_2T_x$ *via* the condensation of amino and car-

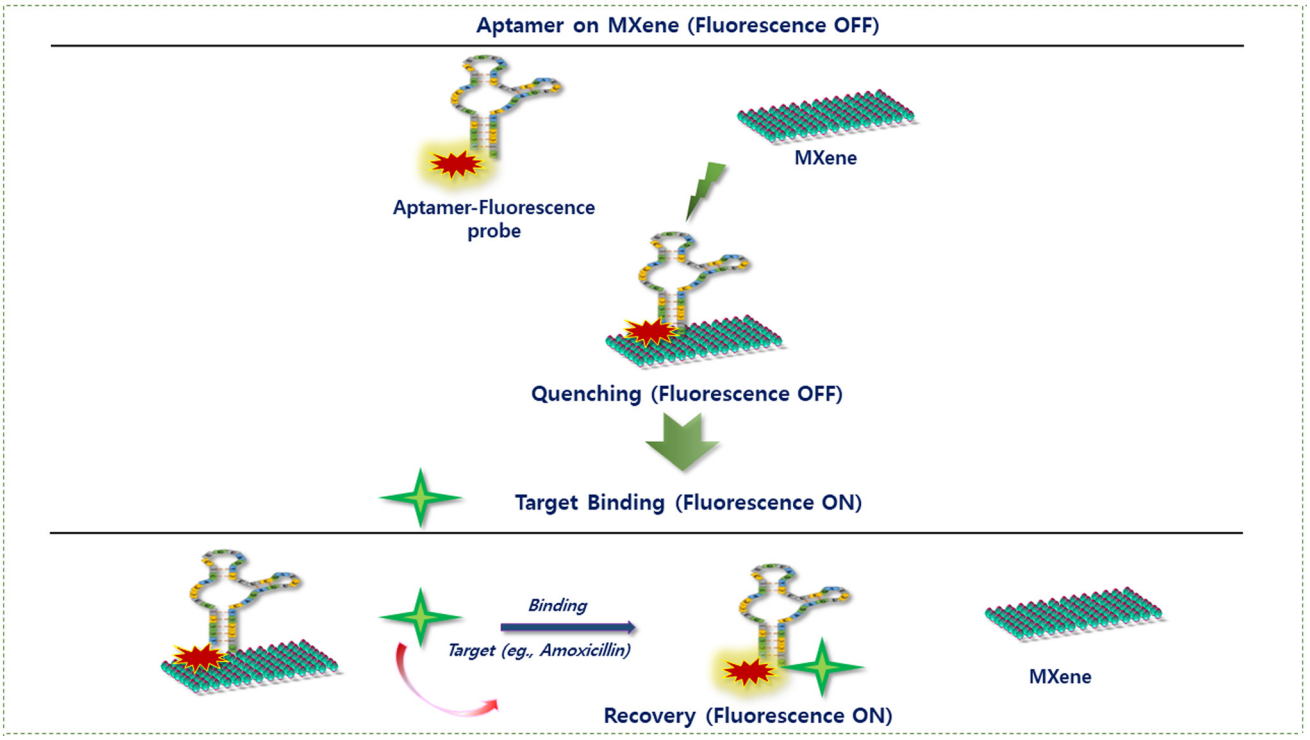

Fig. 3 Schematic illustration of MXene-based aptamer fluorescence sensing.

boxyl groups. The functionalization of MXene sheets with FA-PEG_{2000}-NH_2 serves two primary purposes: FA ligands facilitate binding to folate receptors, which are overexpressed on cancer cell membranes, while PEG enhances the nanoprobe's biocompatibility and stability. The various strategies employed for the functionalization of aptamers on MXene-based platforms are summarized in Table 2.

Surface functionalization not only improves its physicochemical properties it also improves its stability and biocompatibility.[65] Pristine MXene faces challenges such as poor stability in oxygen-rich environments and limited dispersibility in water, often leading to precipitation and aggregation. To address these issues, functionalizing $Ti_3C_2T_x$ flakes with amine molecules has been shown to enhance oxidation resistance and improve the long-term stability of MXene films. Another effective approach involves the functionalization of MXene with thiolated aptamers.[66] These aptamers can form strong bonds with the Ti–F and Ti–OH groups on $Ti_3C_2T_x$, resulting in a densely packed layer of aptamers on the film surface. For instance, a flexible $Ti_3C_2T_x$–aptamer sensing platform was developed to fabricate stable and renewable solution-gated aptamer MXene FET biosensors. In this design, dithiothreitol (DTT), which contains two thiol groups, was first immobilized on the conductive $Ti_3C_2T_x$ film *via* interactions between its –SH groups and the Ti–F or Ti–OH sites. The thiolated aptamer was then linked to this surface through disulfide (–S–S–) bonds, enabling specific target recognition. This strategy also allowed for easy regeneration of the sensing interface, enabling reattachment of either the same or different aptamers. Consequently, multiple FET sensors could be fabricated on a single MXene-based channel, reducing variability between devices caused by using different conductive sub-

Table 2 Summarizes various strategies used for the functionalization of aptamers on MXene-based platforms

Method	Functional group/material	Purpose	Effect of sensing
Surface	–OH, =O groups	Improve hydrophilicity	Enhanced dispersion and fluorescence interaction
Polymer coating	PEG, PVP	Improve biocompatibility	Reduced nonspecific binding, stable signal
Metal nanoparticles	Au, Ag	Enhance the plasmonic effect	Signal amplification, catalytic activity
Doping	N, S, B	Modify the electronic structure	Improved fluorescence or charge transfer
Hybridization	Quantum dots, carbon dots	Create a composite sensor	Enhanced selectivity and sensitivity
Immobilization	Non-covalent adsorption (electrostatic/π–π interactions)	Improve stability	Efficient quenching and target-induced fluorescence recovery

strates. An effective strategy to enhance the fluorescence quenching properties of MXene nanosheets involves incorporating metal ions into their structure. This widely used and reliable approach helps generate highly active aptasensing platforms. Kong *et al.* developed a niobium carbide (Nb_2C) MXene-based aptasensor for aflatoxin detection.[67] In their study, Mn^{2+} ions were introduced onto the surface of Nb_2C-MNs, significantly enhancing both fluorescence quenching efficiency and colorimetric catalytic activity. Various metal ions were tested, and Mn^{2+} exhibited the most significant improvement in the adsorption between Nb_2C-MNs and ssDNA. This enhanced adsorption also strengthened the biosensor's interaction with TMB molecules, further boosting the peroxidase-like catalytic activity of Nb_2C@ssDNA. These modification strategies not only preserve the exceptional properties of MXene but also overcome existing challenges, offering a promising and innovative approach to developing advanced materials with enhanced performance. Additionally, they provide new perspectives and valuable insights for a deeper and more comprehensive understanding of the underlying mechanisms and principles governing material property optimization. In this upcoming session, we will focus on summarizing the fluorescence aptasensors employing MXene nanohybrid in various applications.

5. Applications of MXene-based fluorescent aptasensors

5.1. Detection of biomolecules

Development of advanced biosensors for the early diagnosis of physiological disorders has emerged as a critical area of focus within the biomedical research community. An ideal biosensor must exhibit key attributes such as high reliability, safety, cost-effectiveness, and the ability to produce analytical outputs tailored to specific needs. Among the diverse classes of biosensors, aptamer-based sensors (aptasensors) constructed from single-stranded DNA or RNA oligonucleotides have garnered significant attention due to their exceptional molecular recognition capabilities, high binding affinities, and superior specificity toward a wide range of target analytes, including biomarkers, pathogenic agents, and disease-associated proteins. Recent advancements in MXene aptamer-based fluorescence sensors are summarized in Table 3, and the corresponding aptamer sequences are provided in Table 4 for constructing MXene-based fluorescence sensing platforms.

In a representative study, Cui and colleagues reported the development of a dual-analyte aptasensor for the simultaneous detection of insulin and visceral adipose tissue-derived serine protease inhibitor (vaspin), two clinically relevant biomarkers associated with diabetes mellitus.[68] The sensor design incorporated fluorescein-labelled insulin-binding aptamers (IBAs) and Cy7-labeled vaspin-binding aptamers (VBAs), both anchored to Ti_3C_2 MXene nanosheets. The sensing mechanism was governed by a Förster Resonance Energy Transfer (FRET) process, wherein the fluorescence of the fluorophores was quenched upon proximity to the MXene surface due to energy transfer. Upon specific binding of insulin and vaspin to their respective aptamers, conformational changes in the aptamer structures led to the displacement of the fluorophores away from the Ti_3C_2 surface, resulting in a measurable fluorescence recovery. The strong quenching efficiency and broad-spectrum optical absorption of MXenes significantly enhanced the performance of the aptasensor. The system demonstrated excellent analytical sensitivity, achieving detection limits of 36 pM for insulin and 45 pM for vaspin, with a linear response range spanning 0.1–5 nM. Furthermore, successful application in spiked human serum samples validated the sensor's potential for clinical diagnostics, highlighting the promise of MXene-based platforms for rapid and sensitive biomarker detection.

In another application, the detection of thrombin (coagulation factor IIa), a serine protease pivotal to the blood coagulation cascade and implicated in disorders such as thrombosis, leukemia, Alzheimer's disease, and hepatic dysfunctions, has also benefited from MXene-enhanced aptasensor design. To overcome limitations associated with conventional thrombin assays, Cui *et al.* fabricated a FRET-based aptasensor utilizing a monolayer of Ti_3C_2 MXene as the quenching substrate.[69] In this system, a fluorescently tagged thrombin-specific aptamer was immobilized on the MXene surface *via* hydrogen bonding and chelation interactions between the aptamer's phosphate backbone and surface titanium atoms of the MXene. The proximity of the fluorophore to the Ti_3C_2 surface enabled efficient FRET-mediated quenching. Upon binding to thrombin, the aptamer underwent structural rearrangement, increasing the fluorophore-to-surface distance and restoring fluorescence. This sensor enabled the quantitative detection of thrombin within a concentration range of 0 to 200 pM, with an impressive limit of detection (LOD) of 5.27 pM. These findings underscore the high sensitivity and specificity of Ti_3C_2 MXene-based aptameric platforms, affirming their value as next-generation biosensing tools for clinical and point-of-care diagnostics.

A novel fluorescence-based aptasensor was developed for the ultrasensitive detection of prostate-specific antigen (PSA), a critical biomarker for the early diagnosis of prostate cancer. Given that PSA concentrations in human serum typically fall within the range of 0.4–6.8 mg L^{-1},[70] there is a pressing need for detection platforms with superior sensitivity beyond the capabilities of conventional diagnostic techniques. In this work, the sensing strategy was based on a FRET mechanism, utilizing few-layered V_2CT_x MXene as an efficient fluorescence quencher. The sensor design involved the integration of carboxylated graphene quantum dots (CGQDs) with PSA-specific aptamers functionalized with terminal amino groups.[71] The resulting aptamers CGQD complex was immobilized onto the surface of V_2CT_x MXene *via* electrostatic and π–π stacking interactions, leading to effective fluorescence quenching due to proximity-induced energy transfer. Upon target recognition, binding of PSA to its corresponding aptamer induced a conformational rearrangement, increasing the spatial distance

Table 3 Summary of recent advancements in MXene aptamer-based fluorescence sensor

S. no.	MXene-aptamer probe	Target analyte	Mechanism	Linear range	Limit of detection	Quenching efficiency	Functionalization feasibility	Real-sample matrices	Ref.
1	FAM-IBA and Cy7-VBA/MXene	Insulin and vaspin	FRET	0.1 to 5 nM 0.1 to 5 nM	36 pM 45 pM	Very high	Excellent	Human serum	68
2	TBA/MXene	Thrombin	FRET	20–200 pM	5.27 pM	Very high	Excellent	Human serum	69
3	ssDNA-UCNPs/MXene-Au	Deoxynivalenol (DON)	Luminescence resonance energy transfer	1–500 ng mL^{-1}	0.64 ng mL^{-1}	Very high	Ease and efficiency	Corn flour and Tai Lake water	63
4	POSS-PQDs-Apt	*Vibrio parahaemolyticus* (VP)	FRET	102–106 CFU mL^{-1}	30 CFU mL^{-1}	High	Ease	Seawater	73
5	Aptamer-CGQDs-FL-V_2CT_x	Prostate-specific antigen	PET	0.03 ng mL^{-1}	0.1 to 20 ng /mL	High	Ease	Human serum	71
6	Nb_2C-MXene/B-CDs@Apt	Chloramphenicol Oxytetracycline	FRET (signal on)	1–160 ng mL^{-1}	0.285 ng ml^{-1} (PAD) 0.399 ng mL^{-1} (tube detection) 0.867 ng mL^{-} (PAD)	High	Ease	Human serum	26
7	Ti_3C_2 MXene	Amoxicillin	FRET	100 to 2400 ng mL^{-1}	1.53 ng mL^{-1}	High	Facile	Water bodies	72
8	Nb_2C-MNs	Aflatoxin	Fluorescence quenching	0.1–450 ng mL^{-1}	0.0984 ng mL^{-1}	High	Facile	Peanut samples	74
9	Nb_2C-MXene-GCD labelled aptamers	SARS-CoV-2 spike (S1) protein	FRET	10 ng mL^{-1} to 80 ng mL^{-1}	0.067 ng mL^{-1}	High	Ease	Urban water	75
10	Ti_3C_2MXene sheets	SARS-CoV-2 spike (S1) protein	FRET	0.1 to 100 ng mL^{-1}	38.9 fg mL^{-1}	High	Ease	Clinical sample	76
11	Ti_3C_2MXene sheets	Pb^{2+}	Signal amplification	5.0×10^{-2}–2.0 nmol L^{-1}.	3.7×10^{-2} nmol L^{-1}	High	Facile	Milk and water	77
12	DNA (CQDs–apt–cDNA) and $Ti_3C_2T_x$ flakes	Dimethoate	FRET	1×10^{-9} to 5×10^{-5} M	2.18×10^{-10} M	High	Ease	Apple juice and tap water	78
13	CRISPR/Cas12a $Ti_3C_2T_x$	Aflatoxin B1	Fluorescence on	0.001 to 80 ng m L^{-1}	0.92 pg m L^{-1}	High	Fast and easy	Peanut sample	79

Table 4 Summary of aptamers and their sequences in MXene-based fluorescence sensors

S. no.	Aptamer name	Target analyte	Sequence	Ref.
1	Insulin binding aptamer (IBA)/vaspin-binding aptamer (VBA)	Insulin and vaspin	IBA: 5′-FAM-GGT GGT GGG GGG GGT TGG TAG GGT GTC TTC-3′ VBA: 5′-Cy7-ATA CCA GCT TAT TCA ATT GGG CGG TGG GGG GGG TAG TGG GTG TTA TGG CGA TCG TGG AGA TAG TAA GTG CAA TCT-3′	68
2	Heparin-dependent 1 (HD1) NU172 HD22	Thrombin	HD1: 5′-FAM-GGT TGG TGT GGT TGG-3′. NU172: 5′-FAM-CGC CTA GGT TGG GTA GGG TGG TGG CG-3′ HD22: 5′-FAM-AGT CCG TGG TAG GGC AGG TTG GGG TGA CT-3′	69
3	Deoxynivalenol (DON) aptamer	Deoxynivalenol (DON)	GCA TCA CTA CAG TCA TTA CGC ATC GTA GGG GGG ATC GTT AAG GAA GTG CCC GGA GGC GGT ATC GTG TGA AGT GCT GTC CC	63
4	VP aptamer	*Vibrio parahaemolyticus* (VP)	5′-NH_2-TTTTTTTTTCAACGAAAC AGTGACTCGTTG-3′	73
5	Prostate Specific Antigen (PSA) aptamer	prostate-specific antigen	5′-NH_2-C_6-AATTAAAGCTCGCCATCAAATAGC-3′	71
6	Anti-CAP aptamer/anti-OTC aptamer	Chloramphenicol	5′-NH_2-C_6-CGT ACG GTC GAC GCT AGC TTA GCT TAT GCG TTG GCC GGG ATA AGG ATC CAG CCG TTG TAG ATT TGC GTT CTA ACT CTC CAC GTG GAG CTC GGA TCC-3′	26
		Oxytetracycline	5′-NH_2-C_6-CGT ACG GAA TTC GCT AGC CGA GTT GAG CCG GGC GCG GTA CGG GTA CTG GTA TGT GTG GGG ATC CGA GCT CCA CGT G-3′	
7	Amoxicillin aptamer	Amoxicillin	5′-FAM-TTAGTT GGG GTT CAG TTG G-3′	72
8	Dual-AFB1 aptamers	Aflatoxin	FAM: 5′AAA AAA AAG TTG GGC ACG TGT TGT CTC TCT GTG TCT CGT GCC CTT CGC TAG GCC CAC AC-3′	74
9	SARS-CoV-2 S-RBD aptamer	SARS-CoV-2 spike (S1) protein	5′-NH_2-C_6-CAGCACCGACCTTGTGCTTTGGGAGTGCTGGTCCAAGGGCG TTAATGGACA-3′.	75
10	SARS-CoV-2 S-RBD aptamer	SARS-CoV-2 spike (S1) protein	FAM-5′-ATCCAGAGTGACGCAGCATTTCATCGGGTCCAAAAG GGGCTGCTCGGGATTGCGGATATGGACACGT-3′	76
11	Aptpb	Pb^{2+}	5′-GGTTGGTGTGGTTGG-3′	77
12	Dimethoate-binding aptamer	Dimethoate	5′-NH_2-$(CH_2)_6$-AGC TTG CTG CAG CGA TTC TTG ATC GCC ACA GAG CT-3′ 5′-AGCTCT GTG GCG ATC AAG AAT CGC TGC AG-3′	78
13	AFB1-specific DNA aptamer	Aflatoxin B1	Apt-1 5′-TTGGGCACGTGTTGTCTCTCTGTGTCTCGTGCCCTTCGCTAGGCC CTTGTGT-3′ Apt-2 5′-GTTTGTTGGGCACGTGTTGTCTCTCTGTGTCTCGTGCCCTTCGCT AGGCCC-3′	79

between the fluorophore (CGQD) and the MXene surface, which resulted in fluorescence recovery. The constructed aptasensor demonstrated exceptional sensitivity, achieving a limit of detection (LOD) as low as 0.03 ng mL^{-1}, with a linear dynamic range from 0.1 to 20 ng mL^{-1}. The platform was further validated through the successful detection of PSA in spiked human serum samples, highlighting the sensor's clinical applicability. This study underscores the promising potential of few-layered V_2CT_x MXene as a next-generation fluorescence quencher, offering high surface area, broad-spectrum light absorption, and efficient energy transfer capabilities, thus positioning it as a valuable component in the development of MXene-based fluorescence aptasensing systems.

5.2. Detection of antibiotics

Accurate detection of antibiotics is critical for protecting public health, mitigating the emergence of antimicrobial resistance, and maintaining environmental and food safety. Accordingly, the development of rapid and highly sensitive analytical platforms is essential for monitoring antibiotic residues in clinical, environmental, and agricultural matrices. Zermane *et al.* developed an MXene-based fluorescent aptasensor for detecting amoxicillin (AMOX) in water matrices.[72] The sensor design utilized Ti_3C_2 MXene nanosheets, renowned for their large surface area, high electrical conductivity, and exceptional fluorescence quenching capabilities. A carboxyfluorescein (FAM)-labelled DNA aptamer, specific to AMOX, was immobilized on the MXene surface, serving as the fluorescence energy donor. In the absence of amoxicillin, the proximity between the fluorophore and MXene nanosheets facilitates Förster resonance energy transfer (FRET), leading to efficient fluorescence quenching. When AMOX is present, it binds selectively to the aptamer, inducing a conformational change that increases the distance between the fluorophore and the MXene, thus restoring fluorescence emission. Advanced optimization techniques, including Response Surface Methodology–Central Composite Design (RSM-CCD) and Artificial Neural Network–Genetic Algorithm (ANN–GA), were employed to maximize sensor performance. The developed aptasensor achieved a linear detection range of 100–2400 ng mL^{-1}, with an impressive limit of detection of 1.53 ng mL^{-1}. The method demonstrated excellent reliability and accuracy, highlighting its promising potential for the monitoring of amoxicillin contamination in complex water bodies.

Chloramphenicol, a broad-spectrum antibiotic extensively utilized in veterinary medicine for its protein synthesis inhibition properties, poses significant environmental risks due to its persistence and ecotoxicity, particularly in aquatic ecosystems. Conventional analytical techniques such as high-performance liquid chromatography (HPLC) and liquid chromatography–mass–mass spectrometry (LC–MS), although highly sensitive and specific, are limited by complex sample prepa-

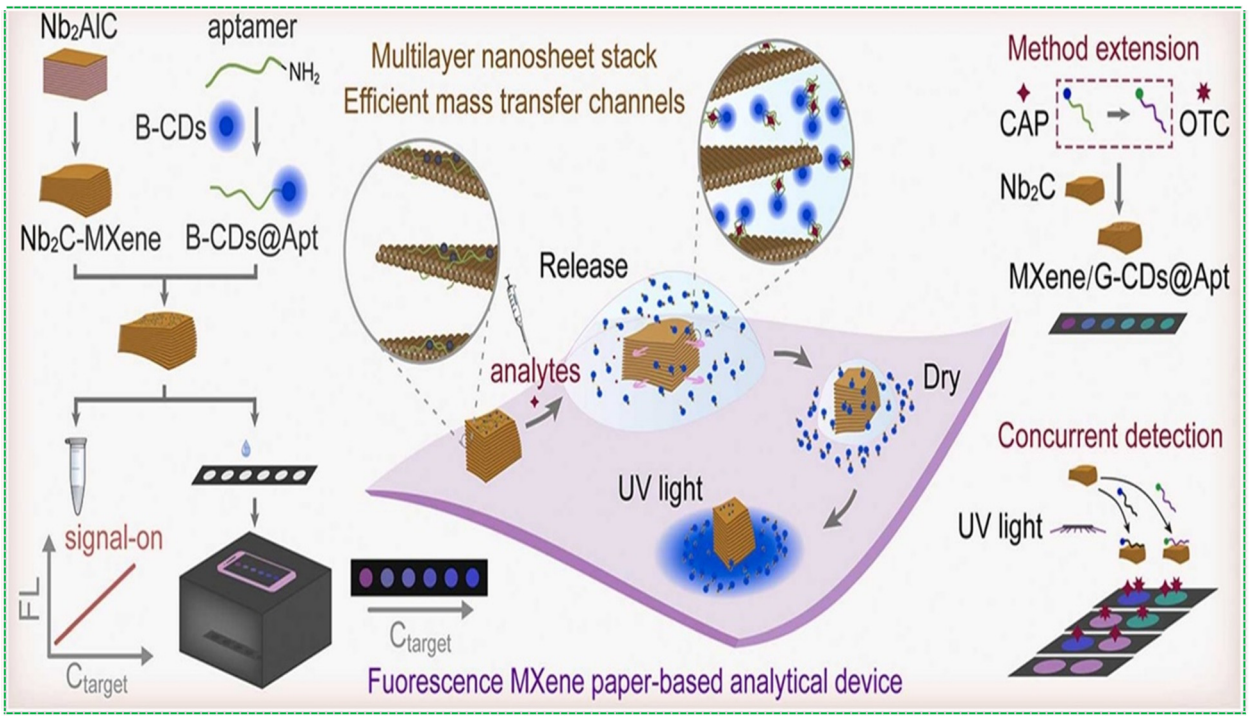

Fig. 4 Schematic diagram for illustrating the preparation of Nb_2C-MXene and B-CDs@Apt and working principle of the Nb_2C-MXene/B-CDs@Apt aptasensor reproduced with permission.[26] Copyright ©2025, Elsevier.

ration, high operational costs, and lack of field-deployable capability. To address these limitations, Yang *et al.* developed a signal-on paper-based fluorescence aptasensor incorporating multilayer niobium carbide MXene (Nb_2C-MXene) as a fluorescence quencher and carbon dots (CDs) as luminescent nanoprobes.[26] In this study, carbon dot-conjugated aptamers (B-CDs@Apt) were employed as molecular recognition elements for the selective detection of chloramphenicol. In the absence of the target analyte, the aptamer-functionalized carbon dots adsorb onto the MXene surface *via* electrostatic interactions and π–π stacking, resulting in efficient fluorescence quenching (signal-off state). Upon specific binding to chloramphenicol, the aptamer undergoes a conformational transition, leading to its desorption from the MXene surface and restoration of fluorescence (signal-on state). The fluorescence intensity exhibited a linear correlation with analyte concentration, enabling quantitative analysis with a detection limit as low as 0.360 ng mL^{-1} on a paper-based substrate. To demonstrate multiplexing capability, the sensing platform was adapted for oxytetracycline (OTC) detection by substituting the aptamer and carbon dot probes, achieving limits of detection of 0.399 ng mL^{-1} in solution and 0.867 ng mL^{-1} on PAD. Fig. 4. illustrates the preparation of Nb_2C-MXene and B-CDs@Apt and the working principle of the Nb_2C-MXene/B-CDs@Apt aptasensor. The integration of MXene-based nanoquenchers with photostable carbon nanoprobes in a portable, paper-based format underscores the potential of this platform for low-cost, rapid, and on-site monitoring of antibiotic residues. These findings highlight the utility of MXene-assisted aptasensors in environmental surveillance and food safety diagnostics.

5.3 Detection of toxin

Aflatoxin B1 (AFB1), a potent mycotoxin produced predominantly by *Aspergillus flavus* and *Aspergillus parasiticus*, is classified as a Group I carcinogen by the International Agency for Research on Cancer (IARC), owing to its strong association with hepatocellular carcinoma.[80] AFB1 contamination in food crops such as maize, peanuts, and grains poses a significant threat to food safety and public health. While conventional analytical methods such as high-performance liquid chromatography (HPLC) and enzyme-linked immunosorbent assays (ELISA) offer high sensitivity and accuracy, their dependence on complex instrumentation, multi-step sample preparation, and extended analysis times limits their suitability for rapid and on-site detection. To address these challenges, Kong *et al.* developed a dual-mode aptamer-based biosensor for the sensitive detection of AFB1, utilizing two-dimensional niobium carbide MXene nanosheets (Nb_2C-MNs) as the sensing platform. The Nb_2C-MNs were engineered *via* Mn^{2+} ion-assisted synthesis, resulting in concave-surfaced nanostructures with enhanced fluorescence quenching and peroxidase-like catalytic activity. The sensor employed FAM-labelled single-stranded DNA aptamers (ssDNA-FAM) as biorecognition elements capable of specifically binding to AFB1.[74] The principle of detecting AFB_1 by Nb_2C@ssDNA was illustrated in Fig. 5. In the fluorescence detection mode, the ssDNA-FAM adsorbed onto the Nb_2C-MNs surface undergoes efficient fluorescence

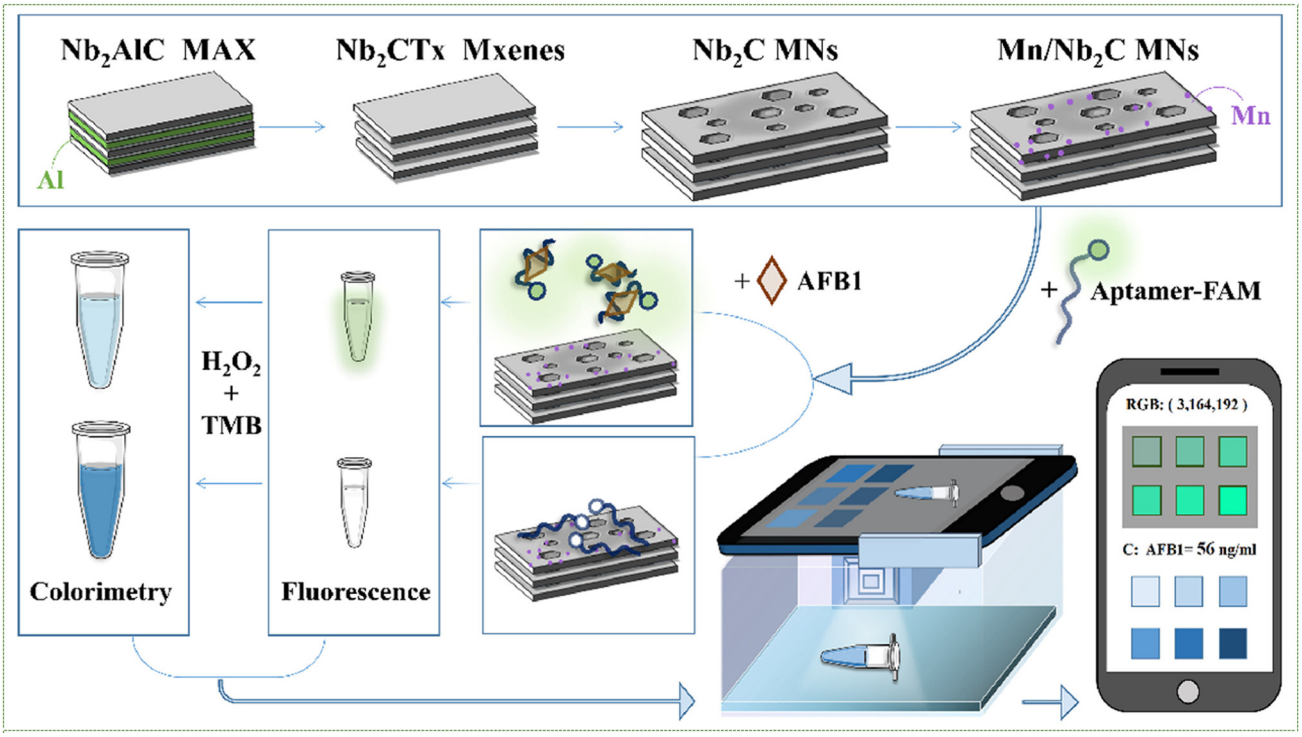

Fig. 5 The principle of detecting AFB_1 by Nb_2C@ssDNA. Reproduced with permission.[74] Copyright ©2023, Elsevier.

quenching. Upon the introduction of AFB1, the aptamer undergoes a conformational change to preferentially bind the target, resulting in its desorption from the nanosheet surface and restoration of fluorescence intensity. In the colorimetric detection mode, the ssDNA-FAM enhances the intrinsic peroxidase-mimetic activity of Nb_2C-MNs. However, the binding of AFB1 attenuates this catalytic activity, leading to a reduction in the colorimetric response. Under optimized conditions, the sensor exhibited a limit of detection (LOD) as low as 0.0950 ng mL^{-1}, along with high specificity and reproducibility. Owing to its dual-mode readout, operational simplicity, and high sensitivity, this biosensor offers significant promise for real-time, on-site monitoring of AFB1 in food safety applications, particularly in resource-constrained or remote environments. Wu *et al.* reported a fluorescence aptamer-based biosensing platform that integrates MXenes with a CRISPR/Cas12a system for the ultrasensitive detection of aflatoxin B1 (AFB1). In this design, dual AFB1-specific aptamers are employed to sequester an activator sequence, while Cas12a is assembled with its corresponding crRNA to form an initially inactive ribonucleoprotein complex. MXenes act as effective adsorption matrices and fluorescence quenchers for FAM-labelled single-stranded DNA (ssDNA-FAM), resulting in pronounced fluorescence suppression. Upon the presence of AFB1, target–aptamer binding induces the release of the activator, thereby triggering Cas12a activation. The activated Cas12a subsequently exhibits nonspecific collateral cleavage toward ssDNA-FAM adsorbed on the MXene surface, leading to fluorescence recovery. The proposed biosensor achieves a wide linear detection range of 0.001–80 ng mL^{-1} with an ultralow detection limit of 0.92 pg mL^{-1} and demonstrates reliable analytical performance in real peanut samples. This platform effectively integrates the molecular recognition specificity of aptamers, the signal amplification capability of CRISPR/Cas12a, and the superior fluorescence-quenching properties of MXenes, enabling highly sensitive AFB1 detection.[79]

5.4. Detection of pathogens

The early, rapid, and accurate detection of bacterial and viral pathogens is of paramount importance for clinical diagnostics, outbreak surveillance, food safety assurance, and environmental monitoring. Although conventional analytical techniques, including culture-based assays, polymerase chain reaction (PCR), and enzyme-linked immunosorbent assays (ELISA), are well established, they are typically labour-intensive, time-consuming, and dependent on specialised infrastructure, thereby limiting their applicability for point-of-care and real-time diagnostics. In contrast, biosensor-based platforms, particularly fluorescence aptasensors, provide compelling alternatives by offering rapid signal transduction, high analytical sensitivity, operational simplicity, and portability.

Vibrio parahaemolyticus, a pathogenic marine bacterium frequently implicated in seafood-borne gastroenteritis, poses a significant public health risk and necessitates sensitive detection strategies. In this regard, Hong *et al.* reported a Ti_3C_2 MXene-based fluorescence resonance energy transfer (FRET) aptasensor, in which MXene nanosheets function as efficient fluorescence quenchers for aptamer-functionalised perovskite

quantum dots.[73] Target-induced aptamer recognition disrupts the MXene–fluorophore interaction, leading to a fluorescence "turn-on" response that enables quantitative detection. The resulting sensing platform achieved a low detection limit of 30 CFU mL^{-1} over a wide linear dynamic range (10^2–10^6 CFU mL^{-1}), demonstrating excellent sensitivity, selectivity, and rapid response. This work underscores the potential of MXene-based fluorescence aptasensors for real-time pathogen detection in food safety and environmental applications.

Since the onset of the COVID-19 pandemic in late 2019, caused by severe acute respiratory syndrome coronavirus 2 (SARS-CoV-2), millions of deaths have been reported globally, highlighting the urgent need for rapid and reliable diagnostic technologies.[81] Reverse transcription polymerase chain reaction (RT-PCR) remains the clinical gold standard owing to its high analytical sensitivity and specificity; however, its reliance on sophisticated instrumentation, skilled operators, and extended assay times constrains its applicability for point-of-care (POC) diagnostics. Although alternative antigen-detection approaches have been reported, limitations related to cost efficiency, operational robustness, and surface-functionalisation complexity have impeded their widespread adoption. MXene-based fluorescence aptasensors have recently emerged as promising platforms to address these challenges. Yang *et al.* developed a paper-based fluorescence aptasensor employing multilayer Nb_2C MXene as an efficient fluorescence quencher and carbon quantum dot-labelled aptamers for the detection of the SARS-CoV-2 spike (S1) protein.[75] Target-induced aptamer binding disrupts MXene-mediated non-radiative energy transfer, generating a fluorescence "signal-on" response with a detection limit of 0.067 ng mL^{-1} in a simple one-step assay format, highlighting its suitability for rapid and low-cost POC screening. The schematic illustration of these developed sensors is shown in Fig. 6. In a related study, Luo *et al.* reported an MXene-based fluorescence aptasensor targeting the spike protein receptor-binding domain, achieving ultra-high sensitivity at the femtogram level and enabling rapid detection of SARS-CoV-2 pseudovirus.[76] Importantly, the sensor was successfully validated using antigen proteins, cultured virus, and clinical nasopharyngeal swab samples, demonstrating high specificity and analytical accuracy. Collectively, these studies underscore the potential of MXene-assisted fluorescence aptasensing platforms to deliver rapid, sensitive, and POC-compatible diagnostics for viral pathogens, supporting their application in pandemic preparedness and infectious disease surveillance.

5.5. Detection of heavy metal ions

The integration of MXenes into aptamer-based fluorescence sensors has opened new avenues for environmental monitoring, particularly for the detection of heavy metals, organic pollutants, and other toxins. In environmental systems, fluorescent aptasensors utilizing MXenes typically operate *via* quenching/dequenching or FRET mechanisms, where a fluorophore-labelled aptamer is adsorbed onto the MXene surface. The fluorescence is quenched due to efficient energy transfer or electron transfer processes between the MXene and the fluorophore. Upon target recognition, such as binding with a specific pollutant (*e.g.*, heavy metal ions like Hg^{2+} or Pb^{2+}, or organophosphates), the aptamer undergoes structural reconfiguration, leading to fluorophore release or increased spatial separation, which in turn restores the fluorescence signal.

One notable research effort focused on the detection of lead ions (Pb^{2+}), which are recognized as hazardous environ-

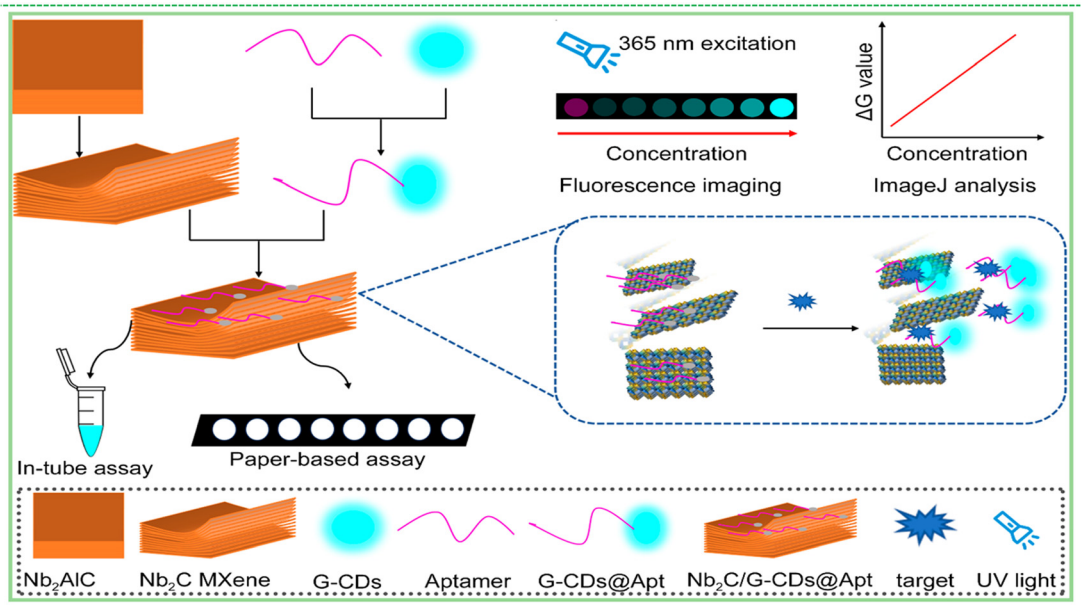

Fig. 6 Schematic of aptamer-based fluorescence paper sensor for SARS-CoV-2 spike protein.[75] Reproduced with permission from MDPI publications under CC BY 4.0 license.

mental pollutants. There is a critical need for simple, rapid, and sensitive methods to detect Pb^{2+} contamination in food products such as milk. In this study, the researchers designed a dual-mode aptasensor that leverages the unique catalytic properties of MXene nanosheets (*e.g.*, Ti_3C_2) combined with the high specificity of Pb^{2+}-binding aptamers, offering both fluorescence and absorbance readouts for robust analytical performance.[77] The sensing mechanism is based on the catalytic oxidation of 3,3′,5,5′-tetramethylbenzidine (TMB) by MXene in the presence of hydrogen peroxide (H_2O_2), producing the oxidized product TMBOX, which exhibits characteristic optical signals. Initially, a Pb^{2+}-specific aptamer adsorbs onto the MXene surface, effectively blocking active catalytic sites and inhibiting its peroxidase-like activity. Upon introduction of Pb^{2+} ions, the aptamer preferentially binds to Pb^{2+}, leading to its detachment from the MXene surface and subsequent restoration of catalytic activity. This results in an increase in both fluorescence and absorption signals, which are quantitatively correlated to the Pb^{2+} concentration. The developed sensor demonstrated remarkable sensitivity, achieving a detection limit as low as 0.05 nmol L^{-1} in milk samples. The aptamer's high binding affinity ensures excellent selectivity towards Pb^{2+}, effectively minimizing interference from other metal ions and matrix components in milk. This approach highlights the dual role of MXenes as both signal transduction elements and catalytic amplifiers, underscoring their potential for robust, selective, and practical environmental pollutant monitoring.

5.6. Detection of pesticides

Dimethoate, a widely used organophosphorus pesticide, is frequently applied for pest control in agricultural practices. However, excessive exposure poses significant health risks, including neurotoxic effects such as depression, cognitive impairment, and anxiety. Conventional analytical techniques, including high-performance liquid chromatography (HPLC)[82] and gas chromatography coupled with mass spectrometry (GC–MS),[83] have been employed for dimethoate detection. Despite their high sensitivity and accuracy, these methods involve labour-intensive sample preparation, expensive instrumentation, and extended analysis time, which limit their utility for rapid and on-site monitoring. In recent years, fluorescence-based sensing platforms have emerged as attractive alternatives due to their rapid response, high sensitivity, and operational simplicity. Among the various fluorescent nanomaterials, carbon quantum dots (CQDs) have garnered significant attention owing to their excellent photostability, tunable photoluminescence, high quantum yield, facile synthesis, and eco-friendly nature. In this context, Li *et al.* developed a fluorescent aptasensor based on a nanocomposite comprising CQDs, dimethoate-specific aptamers, and $Ti_3C_2T_x$ MXene nanosheets.[78] The carboxyl-functionalized CQDs were covalently linked to amino-modified aptamers using carbodiimide-mediated crosslinking chemistry. The schematic illustration for the synthesis, principle, and workflow of the fluorescence aptasensor based on CQDs–apt–cDNA/MXene assemblies for dimethoate detection is shown in Fig. 7(A–D). Subsequent hybridization with complementary DNA (cDNA) resulted in the formation of a CQDs–aptamer–cDNA (CQDs–apt–cDNA) complex. In the absence of dimethoate, the assembled CQDs–apt–cDNA complex interacts with MXene nanosheets *via* fluorescence resonance energy transfer (FRET), leading to efficient quenching of the fluorescence signal. Upon introduction of dimethoate, the aptamer selectively binds to the pesticide, inhibiting its hybridization with cDNA and thus preventing the quenching interaction with MXene. After centrifugation, the dimethoate-bound CQDs remained in the supernatant, resulting in fluorescence signal recovery proportional to the analyte concentration. Under optimized experimental conditions, the aptasensor exhibited a broad linear detection range from 1 × 10–9 to 5 × 10–5 M, with a coefficient of determination (R^2) of 0.996 and an impressively low limit of detection (LOD) of 2.18 × 10–10 M. The sensor also demonstrated excellent recovery performance in real sample matrices such as tap water and apple juice, indicating its strong potential for application in food safety monitoring and environmental analysis. These results highlight the potential of MXene-assisted fluorescence aptasensors as practical tools for pesticide residue monitoring in food and environmental matrices.

5.7 Comparison of MXene with other 2D materials in fluorescence-based aptasesnor

Finally, MXene-based fluorescence aptasensors, as summarized in Table 3, demonstrate excellent analytical performance with low limits of detection across diverse analytes. This high sensitivity can be attributed to their strong fluorescence-quenching capability arising from metallic conductivity and a high electronic density of states, which facilitate efficient non-radiative energy or electron transfer processes (*e.g.*, FRET or PET) and result in favorable signal-to-noise ratios in aptamer-based sensing systems 78. While comprehensive analyte-matched comparisons with other two-dimensional materials such as graphene oxide (GO) and MoS_2 remain limited due to most studies focusing on individual platforms under distinct experimental conditions, the unique electronic properties of MXenes provide a mechanistic basis for their superior analytical sensitivity in many cases. Furthermore, the rich surface chemistry of MXenes, characterized by abundant –O, –OH, and –F terminations, enables versatile chemical functionalization and efficient aptamer immobilization, both of which are crucial for maintaining target-recognition fidelity. Despite these advantages, MXenes, particularly $Ti_3C_2T_x$, are more susceptible to surface oxidation under ambient or aqueous conditions compared to chemically more robust two-dimensional materials. This oxidation can alter surface terminations and diminish electronic conductivity, potentially affecting long-term sensing stability and reproducibility.[84] Nevertheless, numerous MXene-based fluorescence aptasensors have demonstrated reliable performance in complex real-sample matrices, including biological fluids and environmental water samples, highlighting their practical applicability. Overall, while MXenes are not universally superior across all sensing

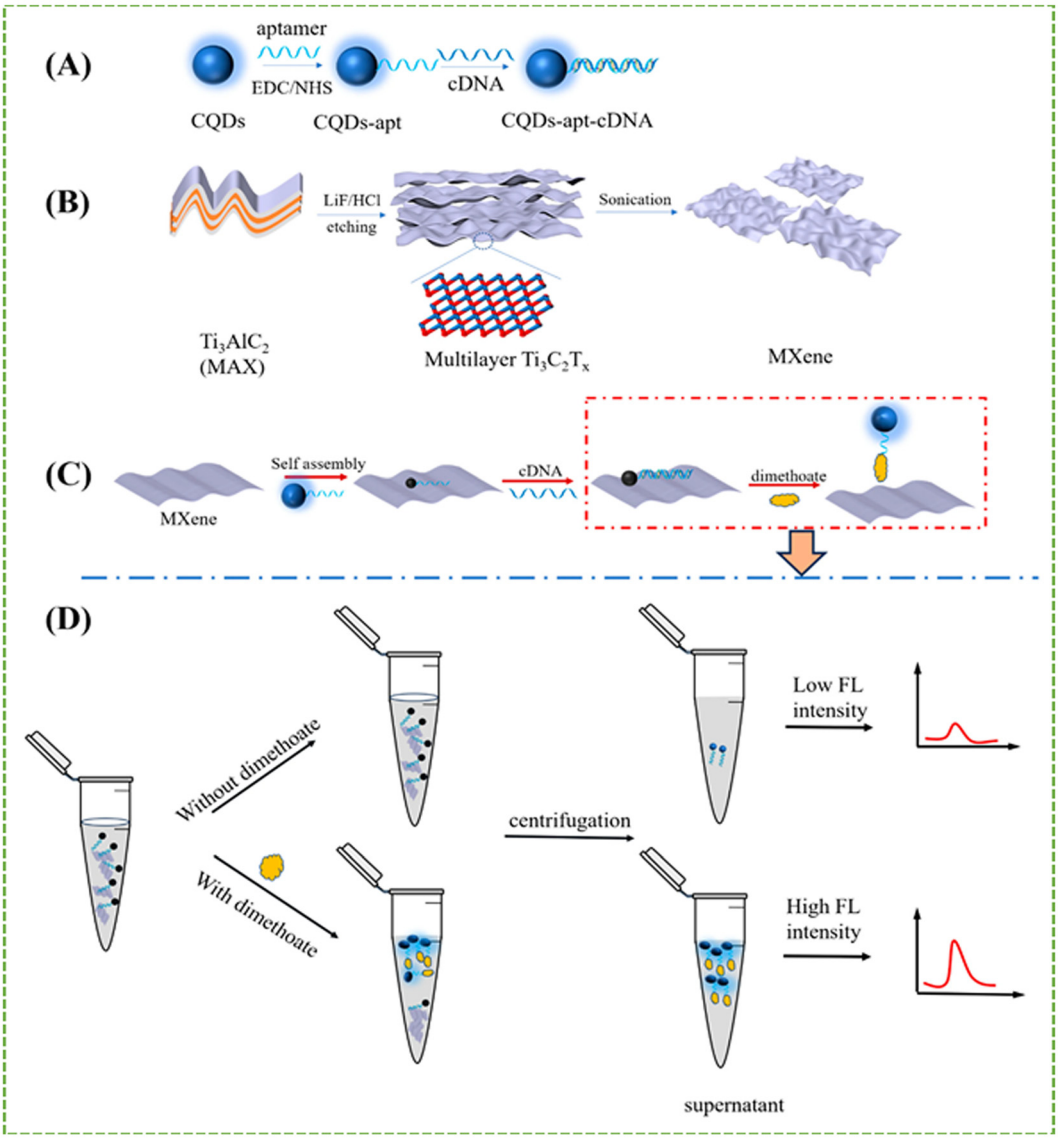

Fig. 7 (A) Schematic illustration of the synthesis route of CQDs–apt and CQDs–apt–cDNA. (B) Schematic illustration of the fabrication of $Ti_3C_2T_x$ flakes. (C) Principle of fluorescence aptasensor for dimethoate determination. (D) Schematic illustration of fluorescence aptasensor based on CQDs–apt–cDNA/MXene assemblies for dimethoate detection.[78] Reproduced with permission from MDPI publications under CC BY 4.0 license.

scenarios, their unique electronic properties and tunable surface chemistry render them a promising platform for high-performance fluorescence aptasensing, provided that stability-related challenges are appropriately addressed.

6. Conclusion and future prospects

MXene-based fluorescence aptasensors constitute an emerging class of high-performance biosensing platforms, wherein the exceptional physicochemical attributes of MXenes namely superior electrical conductivity, tunable surface terminations, and two-dimensional layered architecture are synergistically integrated with the molecular recognition specificity of aptamers. The implementation of advanced surface engineering strategies, including silanization, amine coupling, and heteroatom doping, facilitates stable and oriented aptamer immobilization, thereby enhancing target-binding affinity, sensor robustness, and transduction efficiency. Recent advancements in MXene-based aptasensing systems underscore their remarkable potential for the ultrasensitive detection of clinically relevant biomarkers (*e.g.*, tumor antigens, viral proteins) and environmentally hazardous analytes (*e.g.*, heavy metal ions, organophosphates). Collectively, these findings underscore the promise of MXene–aptamer hybrid platforms as portable and proof-of-concept biosensing systems for point-of-care–oriented diagnostics and real-time environmental surveillance, with full device integration remaining an important direction for future research.

MXene-based fluorescence aptasensors are rapidly emerging as versatile platforms for clinical diagnostics and environmental monitoring. Their unique electrical, optical, and surface properties, combined with aptamer specificity, provide opportunities to develop highly sensitive, selective, and portable sensing technologies. Looking ahead, several research directions and challenges are anticipated to shape their future development:

- **Surface engineering optimization:** employing advanced functionalization methods (*e.g.*, silanization, amine coupling, heteroatom doping) to improve aptamer immobilization, signal transduction, and operational stability.
- **3D architectures and hybrid composites:** constructing three-dimensional MXene frameworks and integrating complementary nanomaterials (*e.g.*, quantum dots, MOFs) to enhance electron transfer, surface area, and fluorescence amplification.
- **Expanding sensing spectrum:** utilizing SELEX-based aptamer design to target novel biomarkers and pollutants, broadening diagnostic and environmental applications.
- **Biomedical deployment:** miniaturizing and integrating sensors into wearable and portable devices for real-time, point-of-care testing.
- **Environmental monitoring:** developing multiplexed sensing arrays capable of simultaneous detection of multiple analytes in complex samples.
- **Smart and connected systems:** combining aptasensors with machine learning, IoT, and wireless communication technologies to create intelligent, autonomous biosensing networks.
- **Material and scalability challenges:** advancing oxidation-resistant surface modifications and establishing reproducible, scalable fabrication protocols for practical applications.
- **Regulatory and biosafety considerations:** conducting systematic evaluations of cytotoxicity, biosafety, and regulatory compliance to support clinical translation and commercialization.

Author contributions

Rajapriya Govindaraju: conceptualization, investigation, formal analysis, writing original draft, editing, and review. Jongsung Kim: validation, investigation, supervision, funding acquisition, formal analysis, and software.

Conflicts of interest

The authors declare no competing financial interest.

Data availability

No primary research results, software or code have been included and no new data were generated or analysed as part of this review.

Acknowledgements

This research was supported by the Core Research Institute Basic Science Research Program through the National Research Foundation of Korea (NRF), funded by the Ministry of Education (No. RS-2021-NR060117), and also supported by the National Research Foundation of Korea (NRF) grant funded by the Korea government (MSIT) (RS-2022-NR069546).

References

1 S. Oncul and A. P. Demchenko, *J. Mol. Recognit.*, 2006, 459–477.
2 S. Y. Lee, N. H. Hairul Bahara, Y. S. Choong, T. S. Lim and G. J. Tye, *J. Colloid Interface Sci.*, 2014, **433**, 183–188.
3 Y. Suzuki and K. Yokoyama, *Biosensors*, 2015, **5**, 337–363.
4 H. Szmacinski and J. R. Lakowicz, *Sens. Actuators, B*, 1995, **29**, 16–24.
5 S. Song, L. Wang, J. Li, C. Fan and J. Zhao, *TrAC, Trends Anal. Chem.*, 2008, **27**, 108–117.
6 J. C. Rosch, D. A. Balikov, F. Gong and E. S. Lippmann, *Eng. Rep.*, 2020, **2**, 1–11.
7 D. Berman, A. Jastrzebska, M. Papi and A. Rosenkranz, *RSC Adv.*, 2024, **14**, 17234–17235.
8 R. K. Sen, P. Prabhakar, N. Bisht, M. Patel, S. Mishra, A. K. Yadav, D. V. Venu, G. K. Gupta, P. R. Solanki, S. Ramakrishnan, D. P. Mondal, A. K. Srivastava, N. Dwivedi and C. Dhand, *Curr. Med. Chem.*, 2021, **29**, 5815–5849.
9 S. S. Sekhon, P. Kaur, Y. H. Kim and S. S. Sekhon, *npj 2D Mater. Appl.*, 2021, **5**, 21.
10 L. Wu, Z. Xu, Q. Meng, Y. Xiao, Q. Cao, B. Rathi, H. Liu, G. Han, J. Zhang and J. Yan, *Anal. Chim. Acta*, 2020, **1099**, 39–45.
11 Z. E. Hughes and T. R. Walsh, *ACS Sens.*, 2017, **2**, 1602–1611.
12 Z. Zhang and H. Karimi-Maleh, *Chemosphere*, 2023, **324**, 138302.
13 W. Wang, S. Xiao, Z. Jia, H. Xie, T. Li, Q. Wang and N. Gan, *Sens. Actuators, B*, 2022, **351**, 130839.
14 I. S. Raja, M. Vedhanayagam, D. R. Preeth, C. Kim, J. H. Lee and D. W. Han, *Int. J. Mol. Sci.*, 2021, **22**(6), 3277.
15 N. Chandrasekar, A. P. Steffi, B. Ramachandran, M. T. Hwang, V. Faramarzi and M. Govarthanan, *Environ. Res.*, 2023, **228**, 115900.
16 R. Akhter and S. S. Maktedar, *J. Materiomics*, 2023, **9**, 1196–1241.
17 Z. Otgonbayar, S. Yang, I. J. Kim and W. C. Oh, *Nanomaterials*, 2023, **13**(5), 919.
18 F. Xie, F. Jia, L. Zhuo, Z. Lu, L. Si, J. Huang, M. Zhang and Q. Ma, *Nanoscale*, 2019, **11**, 23382–23391.
19 R. Govindaraju, J. Paul, J. Kim and J. Kim, *J. Taiwan Inst. Chem. Eng.*, 2026, **179**, 106421.
20 R. Rajamanikandan, K. Sasikumar and H. Ju, *Microchem. J.*, 2026, **220**, 116272.

21 J. Paul and J. Kim, *Appl. Surf. Sci.*, 2023, **613**, 156103.
22 R. Govindaraju, J. Paul and J. Kim, *Microchem. J.*, 2025, **218**, 115744.
23 Y. Jia, T. Wu, G. Wang, J. Jiang, F. Miao and Y. Gao, *Nanomaterials*, 2022, **12**, 2753.
24 A. Kalkal, S. Kadian, S. Kumar, G. Manik, P. Sen, S. Kumar and G. Packirisamy, *Biosens. Bioelectron.*, 2022, **195**, 113620.
25 L. Manzanares, D. Spurling, A. M. Szalai, T. Schröder, E. Büber, G. Ferrari, M. R. J. Dagleish, V. Nicolosi and P. Tinnefeld, *Adv. Mater.*, 2024, **36**, 1–9.
26 J. Yang, M. Liu, J. Wu, T. Ma, Y. Li, Y. Zhang, J. Sun, X. Li, Y. Fang, Y. Wang, L. Cai, Y. Peng, Z. Zhao and J. Bai, *J. Hazard. Mater.*, 2025, **489**, 137720.
27 F. Alshaeer, L. Kareem obeas, M. Zorah, H. A. M. A. Mahmoud, L. M. Abdalgadir, A. G. Taki, B. A. Mohammed, G. Abdulkareem-Alsultan and M. F. Nassar, *J. Alloys Compd.*, 2025, **1011**, 178247.
28 T. Hermann and D. J. Patel, *Science*, 2000, **287**, 820–825.
29 T. Aggarwal, L. Wang, B. Gutierrez, H. Guven, H. Erguven, S. Cho and E. C. Izgu, *Angew. Chem., Int. Ed.*, 2025, **64**, 1–11.
30 P. S. Lau, B. K. Coombes and Y. Li, *Angew. Chem., Int. Ed.*, 2010, **49**, 7938–7942.
31 K. Yoshida, T. Hayashi, M. Takinoue and H. Onoe, *Sci. Rep.*, 2022, **12**, 1–8.
32 D. Yang, X. Liu, Y. Zhou, L. Luo, J. Zhang, A. Huang, Q. Mao, X. Chen and L. Tang, *Anal. Methods*, 2017, **9**, 1976–1990.
33 X. Zhao, T. Gong Liu, H. Chen, X. Chen, L. Zhu, J. Wen and D. Gu, *J. Pharm. Biomed. Anal.*, 2025, **261**, 116820.
34 H. Lee, T. Xie, B. Kang, X. Yu, S. W. Schaffter and R. Schulman, *Nat. Commun.*, 2024, **15**, 1–11.
35 C. Kolm, I. Cervenka, U. J. Aschl, N. Baumann, S. Jakwerth, R. Krska, R. L. Mach, R. Sommer, M. C. DeRosa, A. K. T. Kirschner, A. H. Farnleitner and G. H. Reischer, *Sci. Rep.*, 2020, **10**, 1–16.
36 C. Luo, Y. Lei, L. Yan, T. Yu, Q. Li, D. Zhang, S. Ding and H. Ju, *Electroanalysis*, 2012, **24**, 1186–1191.
37 Y. Lyu, G. Chen, D. Shangguan, L. Zhang, S. Wan, Y. Wu, H. Zhang, L. Duan, C. Liu, M. You, J. Wang and W. Tan, *Theranostics*, 2016, **6**, 1440–1452.
38 K. Sefah, Z. Yang, K. M. Bradley, S. Hoshika, E. Jiménez, L. Zhang, G. Zhu, S. Shanker, F. Yu, D. Turek, W. Tan and S. A. Benner, *Proc. Natl. Acad. Sci. U. S. A.*, 2014, **111**, 1449–1454.
39 J. Yang and M. T. Bowser, *Anal. Chem.*, 2013, **85**, 1525–1530.
40 S. Zhang, Z. Ning, Y. Zhang, X. Lin, N. Duan, Z. Wang and S. Wu, *Biosens. Bioelectron.*, 2025, **271**, 117038.
41 S. Kumar, A. Mohan, N. R. Sharma, A. Kumar, M. Girdhar, T. Malik and A. K. Verma, *ACS Omega*, 2024, **9**, 26838–26862.
42 Y. Wang, L. Bao, Z. Liu and D. W. Pang, *Anal. Chem.*, 2011, **83**, 8130–8137.
43 Q. Qiao, X. Guo, F. Wen, L. Chen, Q. Xu, N. Zheng, J. Cheng, X. Xue and J. Wang, *Front. Chem.*, 2021, **9**, 1–8.
44 H. Zhao, X. Xiang, M. Chen and C. Ma, *Toxins*, 2019, **11**(2), 65.
45 M. Naguib, M. Kurtoglu, V. Presser, J. Lu, J. Niu, M. Heon, L. Hultman, Y. Gogotsi and M. W. Barsoum, *Adv. Mater.*, 2011, **23**, 4248–4253.
46 Z. U. D. Babar, V. Iannotti, G. Rosati, A. Zaheer, R. Velotta, B. Della Ventura, R. Álvarez-Diduk and A. Merkoçi, *Chem. Soc. Rev.*, 2025, **54**, 3387–3440.
47 W. Zhang, S. Li, X. Fan, X. Zhang, S. Fan and G. Bei, *Carbon Energy*, 2024, **6**, 1–25.
48 R. Rajamanikandan, K. Sasikumar and H. Ju, *Environ. Sci. Nano*, 2025, **12**, 4796–4842.
49 R. Govindaraju and J. Kim, *FlatChem*, 2025, **54**, 2452–2627.
50 Z. Li, L. Wang, D. Sun, Y. Zhang, B. Liu, Q. Hu and A. Zhou, *Mater. Sci. Eng., B*, 2015, **191**, 33–40.
51 B. Gurzęda, N. Boulanger, A. Nordenström, C. Dejoie and A. V. Talyzin, *Adv. Sci.*, 2024, **11**, 1–9.
52 L. Liu, M. Orbay, S. Luo, S. Duluard, H. Shao, J. Harmel, P. Rozier, P. L. Taberna and P. Simon, *ACS Nano*, 2022, **16**, 111–118.
53 W. Sun, S. A. Shah, Y. Chen, Z. Tan, H. Gao, T. Habib, M. Radovic and M. J. Green, *J. Mater. Chem. A*, 2017, **5**, 21663–21668.
54 M. Öper, U. Yorulmaz, C. Sevik, F. Ay and N. K. Perkgöz, *J. Appl. Phys.*, 2022, **131**, 025304.
55 X. Xiao, H. Yu, H. Jin, M. Wu, Y. Fang, J. Sun, Z. Hu, T. Li, J. Wu, L. Huang, Y. Gogotsi and J. Zhou, *ACS Nano*, 2017, **11**, 2180–2186.
56 Z. Zhang, F. Zhang, H. Wang, C. Ho Chan, W. Lu and J. Y. Dai, *J. Mater. Chem. C*, 2017, **5**, 10822–10827.
57 H. Shin, W. Jeong and T. H. Han, *Nat. Commun.*, 2024, **15**, 10507.
58 A. Parveen, D. Tyagi, V. Laxmi, N. Ullah, F. Ahmad, A. Irshad, K. Tao and Z. Ouyang, *Materials*, 2025, 1–18.
59 D. Ontiveros, F. Viñes and C. Sousa, *J. Mater. Chem. A*, 2023, **11**, 13754–13764.
60 M. Mozafari and M. Soroush, *Mater. Adv.*, 2021, **2**, 7277–7307.
61 A. N. Kumar and K. Pal, *Mater. Adv.*, 2022, **3**, 5151–5162.
62 H. Zhang, Z. Wang, Q. Zhang, F. Wang and Y. Liu, *Biosens. Bioelectron.*, 2019, **124–125**, 184–190.
63 X. Lin, C. Li, X. Meng, W. Yu, N. Duan, Z. Wang and S. Wu, *J. Hazard. Mater.*, 2022, **433**, 128750.
64 X. Guan, J. Wang, G. Qi, L. Chen, B. Wang and Y. Jin, *Anal. Chem.*, 2025, **97**, 2770–2778.
65 J. Yoon, S. Kim, K. H. Park, S. Lee, S. J. Kim, H. Lee, T. Oh and C. M. Koo, *Small Methods*, 2023, **7**, 1–11.
66 J. Liu, F. Tan, T. Cao, R. Yu and Y. Wang, *Biosens. Bioelectron.*, 2025, **271**, 117096.
67 Y. Kong, Z. Li, L. Zhang, J. Song, Q. Liu, Y. Zhu, N. Li, L. Song and X. Li, *Biosens. Bioelectron.*, 2023, **242**, 115725.
68 H. Cui, L. Yang, X. Fu, G. Li, S. Xing and X. F. Wang, *Surf. Interfaces*, 2023, **41**, 103196.
69 H. Cui, X. Fu, L. Yang, S. Xing and X. F. Wang, *Talanta*, 2021, **228**, 122219.

70 S. Goč and M. Janković, *J. Med. Biochem.*, 2017, **36**, 322–330.
71 T. Zhu, Q. Tang, Y. Zeng, S. Chen, Y. Yang, H. Wang, J. Chen, L. Guo and L. Li, *Spectrochim. Acta, Part A*, 2023, **293**, 122474.
72 M. Zermane, M. Berkani, A. Teniou, T. M. Aminabhavi, Y. Vasseghian, G. Catanante, N. Lakhdari and A. Rhouati, *J. Environ. Manage.*, 2024, **360**, 121072.
73 J. Hong, W. Wang, J. Wang, X. Wang, H. Xie, T. Li and N. Gan, *Microchim. Acta*, 2021, **188**, 45.
74 Y. Kong, Z. Li, L. Zhang, J. Song, Q. Liu, Y. Zhu, N. Li, L. Song and X. Li, *Biosens. Bioelectron.*, 2023, **242**, 115725.
75 J. Yang, Z. Zhao, T. Ma and J. Bai, *Sensors*, 2025, **25**, 1–15.
76 Y. Luo, X. Jiang, R. Zhang, C. Shen, M. Li, Z. Zhao, M. Lv, S. Sun, X. Sun and B. Ying, *Small*, 2023, **19**, 1–6.
77 S. Zhi, Q. Wei, C. Zhang, C. Yi, C. Li and Z. Jiang, *Front. Nutr.*, 2022, **9**, 1008620.
78 Z. Li and H. Pu, *Biosensors*, 2024, **14**, 69.
79 Z. Wu, D. Sun, H. Pu and Q. Wei, *Talanta*, 2023, **252**, 123773.
80 Q. Zhu, Y. Ma, J. Liang, Z. Wei, M. Li, Y. Zhang, M. Liu, H. He, C. Qu, J. Cai, X. Wang, Y. Zeng and Y. Jiao, *Signal Transduction Targeted Ther.*, 2021, **6**, 1–13.
81 P. Jha, P. E. Brown and R. Ansumana, *Lancet*, 2022, **399**, 1937–1938.
82 B. A. Khan, A. Farid, M. R. Asi, H. Shah and A. K. Badshah, *Food Chem.*, 2009, **114**, 286–288.
83 E. Gallardo, M. Barroso, C. Margalho, A. Cruz, D. N. Vieira and M. López-Rivadulla, *Rapid Commun. Mass Spectrom.*, 2006, **20**, 865–869.
84 C. Rawat, S. Shaikh, M. R. Hasan, D. Naithani, S. Singh, P. Sharma, E. G. Celik, S. Timur, R. Pilloton and J. Narang, *ACS Appl. Mater. Interfaces*, 2024, **16**, 24514–24524.